

INVESTIGATION OF PHOTOVOLTAIC PERFORMANCE OF DYE-SENSITIZED  
SOLAR CELL USING TIN (IV) OXIDE IN DIFFERENT  
MORPHOLOGIES AS SEMICONDUCTOR

By

Bach Song Pham

Submitted in partial fulfillment of the requirements for  
Departmental Honors in the Department of Chemistry and Biochemistry  
Texas Christian University  
Fort Worth, Texas

December 16, 2019

INVESTIGATION OF PHOTOVOLTAIC PERFORMANCE OF DYE-SENSITIZED  
SOLAR CELL USING TIN (IV) OXIDE IN DIFFERENT  
MORPHOLOGIES AS SEMICONDUCTOR

Project Approved:

Supervising Professor: Benjamin Sherman, Ph.D.

Department of Chemistry and Biochemistry

Kayla Green, Ph.D.

Department of Chemistry and Biochemistry

Jeffrey Roet, Ph. D.

Department of Geography

## ABSTRACT

The dye-sensitized solar cells (DSSCs) are a possible alternative tool to harvest solar energy instead of the traditional silicon-based solar cells. DSSCs offer various advantages, such as good energy conversion efficiencies in low-light condition, simple fabrication, low cost, and the ability to modify key properties of the solar cell such as the absorbance wavelengths. We are interested in developing new types of semiconductor supports for use in DSSCs based on tin(IV) oxide nanoparticles (NPs). Compared with the more widely used titanium dioxide, tin(IV) oxide offers a wider band gap and higher electron mobility, which increase the photostability of the cell and minimize electron energy loss during transport. In this study, two morphologies of tin(IV) oxide, spherical and flower-like NPs, are synthesized. These two types of tin(IV) oxide NPs and mixtures of both at various ratios are used to fabricate DSSCs. We find that nanoflowers usually give the cells higher open circuit voltages but with lower photocurrent. Nanospheres give much higher photocurrent but with lower open circuit voltage. A mixture that has a 2:1 molar ratio of nanoflowers and nanospheres gave the best performance in terms of photocurrent and voltage. Moreover, this project also investigates possible modification of the tin(IV) oxide-based DSSCs which could potentially increase the performance of the solar cells even further. Two approaches are the introduction of a blocking layer on the FTO glass underneath the semiconducting material and the deposition of a titanium oxide coating directly on the tin(IV) oxide semiconducting layer of the solar cells. Both approaches show significant improvement in photovoltaic performance. Together with the encouraging results from the mixture of the tin(IV) oxide nanospherical particles and nanoflowers as semiconducting materials for DSSCs, these approaches are promising in the optimization of DSSCs in the future.

## ACKNOWLEDGEMENT

I have a wonderful opportunity, as an international student, to attend Texas Christian University, and I have never doubted my decision to come here to Fort Worth. My overall at TCU experience is incredibly great, and it is even better with the people I have met and have the chance to work with. I would like to express my special acknowledgement to Dr. Benjamin Sherman, whose guidance as both my research advisor, mentor, and course instructor has helped me to improve myself as a student, a researcher, and a writer. In addition to Dr. Sherman, I would also like to acknowledge the faculty members at TCU, especially Dr. Kayla Green and Dr. Benjamin Janesko from the Department of Chemistry and Biochemistry, and Dr. Jeffrey Roet from the Department of Geography, for being amazing mentors and helping me hone my writing and critical thinking skills, among others. I also want to thank the members of Dr. Sherman's research group for always being willing to assist me in and out of the laboratory. Last but not least, I would like to thank the John V. Roach Honors College and the Department of Chemistry and Biochemistry at TCU for giving me an opportunity to work on an innovative research project and present my hard work, dedication, and ideas to the public.

**TABLE OF CONTENT**

<b>LIST OF FIGURES .....</b>	<b>1</b>
<b>LIST OF TABLES .....</b>	<b>2</b>
<b>INTRODUCTION .....</b>	<b>3</b>
<b>Potential of Solar Energy .....</b>	<b>3</b>
<b>Dye-sensitized Solar Cells .....</b>	<b>4</b>
<b>Semiconductors for DSSCs .....</b>	<b>9</b>
<b>Tin(IV) Oxide as Semiconductor for DSSC .....</b>	<b>10</b>
<b>EXPERIMENTAL .....</b>	<b>12</b>
<b>RESULTS .....</b>	<b>15</b>
<b>SEM Images of SnO<sub>2</sub> Spherical Nanoparticles and Nanoflowers .....</b>	<b>15</b>
<b>TEM images and EDS analysis of SnO<sub>2</sub> spherical particles and flower-like particles.....</b>	<b>16</b>
<b>Visual Inspection of Photoanodes .....</b>	<b>18</b>
<b>UV-Visible Spectra of Photoanodes .....</b>	<b>18</b>
<b>Photovoltaic Performance of DSSCs .....</b>	<b>19</b>
<b>DISCUSSION .....</b>	<b>22</b>
<b>Characteristics of SnO<sub>2</sub> Particles .....</b>	<b>22</b>
<b>Characteristics of Photoanodes .....</b>	<b>23</b>
<b>Photovoltaic Performance of Dye-sensitized Solar Cells .....</b>	<b>27</b>
<b>CONCLUSION .....</b>	<b>32</b>
<b>REFERENCES .....</b>	<b>35</b>

## LIST OF FIGURES

<b>Figure 1.</b> An overall scheme of a DSSC and its simplified operating principle. ....	6
<b>Figure 2.</b> An example of a J-V curve (red curve) .....	8
<b>Figure 3.</b> Chemical structure of N719 dye used in this experiment to fabricate DSSCs .....	12
<b>Figure 4.</b> SEM images of SnO <sub>2</sub> NFs at different magnification .....	16
<b>Figure 5.</b> TEM images of SnO <sub>2</sub> NFs and NPs at different magnification. ....	17
<b>Figure 6.</b> EDS spectra of SnO <sub>2</sub> NPs and SnO <sub>2</sub> NFs .....	17
<b>Figure 7.</b> Images of photoanodes using different semiconducting materials. ....	18
<b>Figure 8.</b> UV-Vis spectra of undyed and dyed DSSC photoanodes. ....	19
<b>Figure 9.</b> Representative J-V curves of DSSC.....	20
<b>Figure 10.</b> Representative J-T plots of DSSCs .....	21
<b>Figure 11.</b> SEM cross-sectional images of FS21-based photoanodes that has not undergo TiO <sub>2</sub> treatment and has undergo TiO <sub>2</sub> treatment.....	31

## LIST OF TABLES

<b>Table 1:</b> Atomic and weight composition of SnO <sub>2</sub> NPs and NFs from EDS analysis.....	16
<b>Table 2:</b> Average values of photovoltaic parameters generated by DSSCs.....	21

## INTRODUCTION

### Potential of solar energy

In a world where fossil fuels continue to be human's dominant source of energy, mankind is running into an unprecedented problem. The fossil fuel used by most industrial and household processes, usually made of hydrocarbon, emits carbon dioxide gas, which is the primary cause of greenhouse effect and global warming. From 1880 to 2010, carbon dioxide content in the atmosphere has risen from 289.8 ppm to 388.4 ppm, and that is a 34% increase in just over 100 years.<sup>1</sup> The consequences are serious climate changes happening globally which threaten the ecosystem and human activities. Therefore, it is imperative to develop alternative and renewable energy sources before humanity faces an energy crisis. Potential candidates such as wind power, hydropower, geothermal energy, biofuel, and solar energy are currently being examined rigorously in hope of finding a viable replacement for fossil fuels. Among these alternatives, solar energy stands out as exceptionally promising.

The Sun has been a constant supplier of energy for Earth since the planet's formation. Around  $3 \times 10^{24}$  J of energy from the Sun reaches the Earth's surface every day, which is about ten thousand times higher than daily global consumption.<sup>2</sup> In other words, if solar conversion devices with 10% efficiency are installed in 0.1% of the Earth surface, they could provide enough energy to fulfill global demand. These numbers show the huge potential of solar energy, and they encourage the scientific community to devise many methods to harness this limitless source of power. Most of solar energy harvesting devices are based on the photovoltaic effect, discovered in 1839 by Alexander-Edmond Becquerel.<sup>3</sup> Materials that exhibit the photovoltaic effect create voltage and electric current upon exposure to light, and scientists can exploit this to create solar cells. The first modern solar cell was made by Russell Ohl in 1946,<sup>3</sup> and since then there have been

many versions of solar cells using different types of materials and different setup. As of now, solar cells are categorized into three groups: first generation, second generation, and third generation. First-generation solar cells are based on silicon wafers, and they are currently the most popular type of solar devices due their high conversion efficiencies.<sup>4</sup> Most of the commercial solar panels used in household are made of first-generation solar cells. Second-generation solar cells utilize thin-film technology, which allows a thin monolayer of photovoltaic material to be deposited on a surface such as glass.<sup>5</sup> This type of solar cell provides more flexibility and economical benefits even though its efficiency is lower than the silicon-based solar cells. Third-generation solar cells are a group of relatively new types of solar cells that have high upsides but have yet to be commercially available.<sup>3</sup> Among this group are the dye-sensitized solar cells, which are usually considered to be the most promising technology in harvesting solar energy and are the main target for investigation in this paper.

### **Dye-sensitized solar cells**

Dye-sensitized solar cells (DSSCs) are among the newest devices designed to harvest solar energy. The first DSSCs were fabricated by Michael Gratzel and Brian O'Regan in 1991,<sup>6</sup> thus DSSCs are sometimes called Gratzel cells. The device Gratzel and O'Regan constructed consisted of a transparent film of titanium(IV) oxide nanoparticles with a coating of photosensitive dye. DSSC has emerged as a very promising technology due to their many advantages over the traditional silicon-based solar cells. Due to its relatively cheap components and its respectable performance, a DSSC is more cost-effective than most other types of solar cells.<sup>7</sup> Moreover, it is easy to fabricate, and thus DSSC has appealing commercial processability using automated manufacturing. The flexibility of a DSSC is also remarkable as researchers could use many different combinations of materials to construct the cells.<sup>8</sup> It is true that as of right now, the highest

solar energy conversion efficiency for DSSC is only half of that of state-of-the-art silicon-based solar cell.<sup>9</sup> However, it possesses distinctive characteristics that can be utilized in ways the silicon-based solar cell cannot. An example is its excellent performance in low or diffused light, which promote its application in indoor settings, shaded regions, and in cloudy weather.<sup>10</sup> All these upsides and potential make DSSCs a leading candidate in the field of photoelectrochemistry going forward.

Dye-sensitized solar cells are relatively simple to fabricate. A dye-sensitized solar cell system has four main components.<sup>11</sup> The first part is photoanode consisting of a mesoporous metal oxide thin layer deposited on a transparent conductive glass surface. The second part is a monolayer of photosensitive dye molecules that are covalently bonded to the surface of the metal oxide layer. This photosensitive dye is the main component that harvest light and generated photoexcited electrons. The third part is a counter electrode usually made of a transparent conductive glass substrate coated with platinum. The final part is an electrolyte solution between the photoanode and the counter electrode containing a redox couple (usually the  $I^-/I_3^-$  redox pair) to collect electrons at the counter electrode and regenerate the oxidized dye.

A schematic structure of a dye-sensitized solar cell and its simplified operating principle is shown in Figure 1.

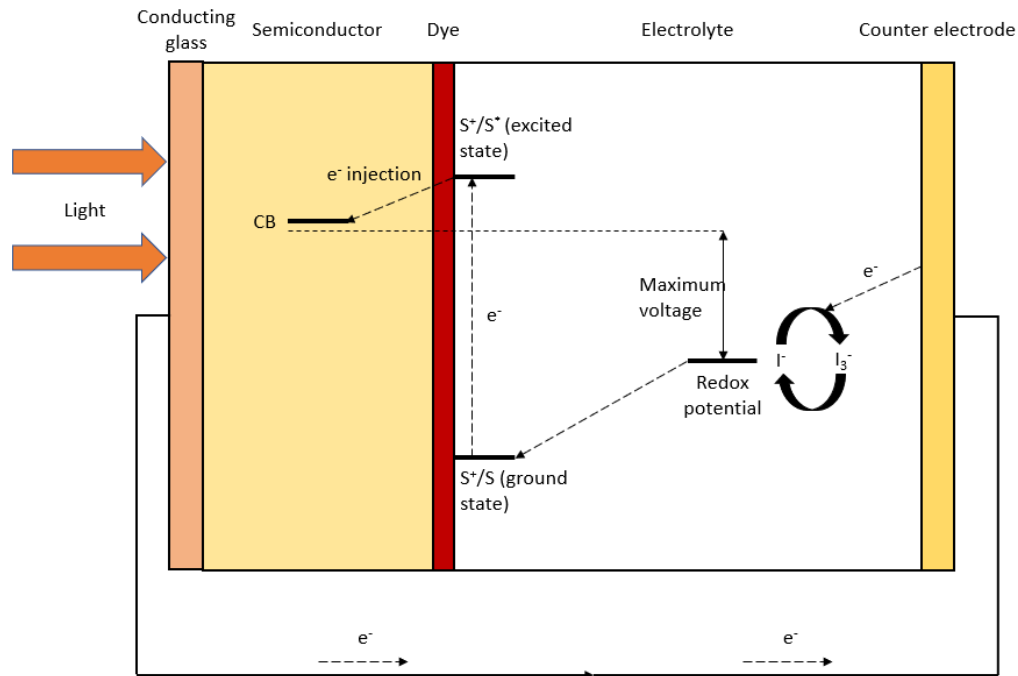


**Figure 1.** An overall scheme of a DSSC and its simplified operating principle. Four main components are shown in the figure: a photoanode made of a mesoporous metal oxide layer (in this case TiO<sub>2</sub>) deposited on a transparent conducting glass surface, a monolayer of photosensitive dye, an electrolyte solution, and a counter electrode. The flow of electrons in the system is indicated by blue arrows. Important energy levels in the system are also shown, and the maximum voltage is shown to be the difference between the redox potential of the electrolyte and the Fermi level of the metal oxide.

The operation principle of a DSSC comprises of four basic steps as follow.<sup>12</sup> First, the incident photons from the sun reach the DSSC and are absorbed by the photosensitive dye. Due to this photon absorption, the electrons are promoted from their ground states to excited states. Then, the excited electrons are then injected into the conduction band (CB) of the mesoporous metal oxide semiconductor. Since the CB of the semiconductor has a lower energy level than that of the excited state of the dye, the process is thermodynamically favorable. The dye is oxidized due to

the loss of electrons. In the next step, the injected electrons diffuse through the metal oxide layer, reach the transparent conductive glass substrate in the back of the photoanode, and subsequently reach the counter electrode through the external circuit. Finally, the electrons at the counter electrode reduce  $I_3^-$  in the electrolyte solution to  $I^-$ . This drives the dye regeneration to take place due to the acceptance of electrons from the  $I^-$  redox mediator, and  $I^-$  gets oxidized to  $I_3^-$ . The  $I_3^-$  diffuses towards the counter electrode and get reduced again to  $I^-$  by incoming electrons from the photoanode.

The movement of electrons in the DSSC system facilitated by sunlight generates power that could be harnessed and utilized to do useful work. The overall performance of the DSSC are characterized by several key parameters,<sup>11</sup> with the sunlight-to-electric power conversion efficiency ( $\eta$ ) being the most crucial one. The parameter  $\eta$  is defined by eq 1:

$$\eta = \frac{P_{\max}}{P_{\text{in}}} \quad (1)$$

with  $P_{\max}$  being the maximum power generated by the solar cell, and  $P_{\text{in}}$  being the power of the incident light. Two other important parameters of DSSCs are the open circuit photovoltage ( $V_{\text{OC}}$ ) and the short circuit photocurrent density ( $J_{\text{SC}}$ ).  $V_{\text{OC}}$  is the theoretical maximum potential difference generated by the cell under illumination and is defined by the difference of the Fermi level of electrons in the metal oxide semiconductor and the redox potential of the electrolyte.<sup>13</sup>  $J_{\text{SC}}$  is the theoretical maximum current possibly produced by the solar cell and is given by the light harvesting efficiency of the dye, its capacity to inject electrons into the metal oxide CB, and the ability of the metal oxide to transport them to the collecting electrode. The ratio between  $P_{\max}$  and the product of  $V_{\text{OC}}$  and  $J_{\text{SC}}$  is called the fill factor (FF) of the solar cell and is usually presented as a percentage.

$$FF = \frac{P_{\max}}{V_{OC} \times J_{SC}} \times 100\% \quad (2)$$

The fill factor is a measure of quality of the cell and is affected by the cell's shunt resistance and series resistance.<sup>14</sup> It compares the maximum available power of the cell to its maximum theoretical power.  $P_{\max}$ ,  $V_{OC}$ ,  $J_{SC}$ , and FF could be graphically shown in a J-V curve of a solar cell; an example of a J-V curve is depicted in Figure 2.

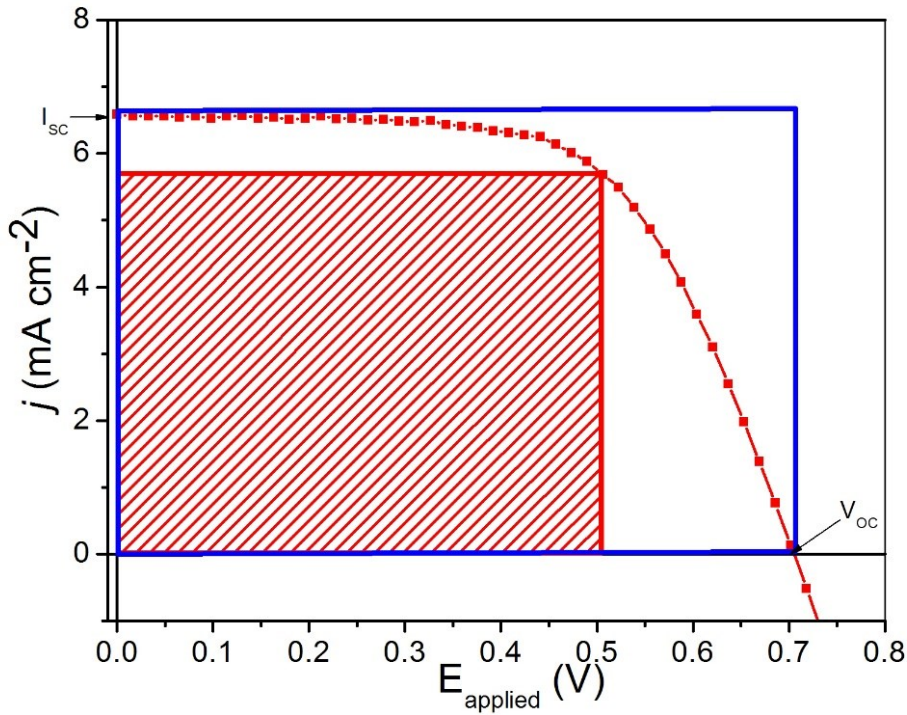


**Figure 2.** An example of a J-V curve (red curve), with  $I_{SC}$  and  $V_{OC}$  indicated on the axes. The red shaded rectangle area represents  $P_{\max}$ , whereas the area of the blue rectangle is the product of  $I_{SC}$  and  $V_{OC}$ . The fill factor is the area of the red rectangle divided by the area of the blue rectangle.

By evaluating these key parameters, scientists could ameliorate the performance of DSSCs by modifying the components of the cell. Due to a myriad of materials that are suitable for the construction of DSSCs, scientists consider this solar energy harvesting system as tremendously promising.

## Semiconductors for DSSCs

Unlike semiconductors in the traditional silicon-based solar cell, which perform both light absorption and charge-carrier transport, the thin layer of semiconductor in DSSC only function as an electron transport system.<sup>15</sup> By having the two functions separately controlled by different components, DSSCs offer impressive flexibility in choices of material. At the present time, state-of-the-art DSSCs use titanium(IV) oxide ( $\text{TiO}_2$ ) as the metal oxide semiconductor. For a DSSC to function optimally, the materials used to make the metal oxide semiconductor layer must meet certain requirements.<sup>8</sup> First, the metal oxide film needs to be mesoporous in order to absorb a large amount of dye. Second, the metal oxide must possess high electron mobility to support effective electron transport through the thin film and to curtail electron energy loss during transport. Finally, the material must possess an electronic band structure with suitable energy levels. The electronic energy level of the metal oxide should maximize the gradient in the Fermi levels of the materials across which the electron flows while minimize the energy loss, which mainly comes from the difference of the conduction band minimum of the metal oxide and the lowest unoccupied molecular orbital (LUMO) of the dye.

The optimal materials for a DSSC should possess these characteristics, and scientists have found that, so far,  $\text{TiO}_2$  offers the highest photovoltaic performance. It is currently the semiconductor of choice for DSSC construction. However,  $\text{TiO}_2$  itself has some inherent disadvantages that are hard to overcome. The salient drawback of  $\text{TiO}_2$  lies in its slow electron diffusion and relatively low electron mobility compared to other materials.<sup>16</sup> Attempts to circumvent this problem involve the synthesis of one-dimensional  $\text{TiO}_2$  nanostructures such as nanorods, which improve the electron mobility of the material.<sup>17,18</sup> Nevertheless, this approach creates another problem: these structures have lower surface areas that reduces the ability of the

cell to adsorb dye; thus, the solar conversion efficiency ( $\eta$ ) is restricted. These disadvantages provide remarkable barriers to ameliorate the DSSC technology that is based on  $\text{TiO}_2$ .

The aforementioned obstacles have redirected the scientific community to alternative materials such as zinc oxide ( $\text{ZnO}$ ) and tin(IV) oxide ( $\text{SnO}_2$ ).  $\text{SnO}_2$  particularly stands out due to its various advantages that could be exploited. Of course, it also possesses many undesirable characteristics that limit its use in a conventional DSSC system. However, attempts to circumvent these problems have been researched by many groups and have produced optimistic results. This project also tackles the disadvantages of  $\text{SnO}_2$  by investigating the use of  $\text{SnO}_2$  in different morphologies as semiconductor for a DSSC.

#### **Tin(IV) oxide as semiconductor for DSSC:**

$\text{SnO}_2$  has garnered a lot of attention from scientists in the field of photoelectrochemistry in recent years.<sup>8</sup> It is a promising material due to its great upsides and its manageable drawbacks. The main advantage that  $\text{SnO}_2$  has over  $\text{TiO}_2$  is much greater electron mobility, and a higher electron mobility allows the DSSC to minimize interfacial charge recombination losses to oxidized redox species in the electrolyte solution.<sup>19</sup> However,  $\text{SnO}_2$ -based DSSCs still have inferior performance compared to their  $\text{TiO}_2$ -based counterparts because of the inherent disadvantages of the material. The first challenge for  $\text{SnO}_2$ -based DSSCs are their inferior dye loading capacities that lead to lower  $J_{\text{SC}}$ . This is due to the lower isoelectric point of  $\text{SnO}_2$  (pH 4-5) compared to that of anatase  $\text{TiO}_2$  (pH 6-7).<sup>20</sup> The second challenge is the more positive CB edge of  $\text{SnO}_2$  compared to that of  $\text{TiO}_2$  that increases the overpotential of the system (i.e. more power loss) and promotes more charge recombination of the excited electrons with the reduced dye molecules and redox species (i.e. lower  $V_{\text{OC}}$ ).<sup>21,22</sup> Many research groups have found innovative methods to minimize these effects on the overall performance of the DSSC, and one of these approaches is the synthesis of

SnO<sub>2</sub> in multidimensional morphologies to use in the fabrication of the DSSC instead of the more traditional spherical nanoparticles.

SnO<sub>2</sub> used in DSSCs initially takes the form of spherical nanoparticles (NP) that have diameters ranging from 10 nm to 40 nm. These nanoparticles could be easily synthesized using a simple hydrothermal treatment with a SnO<sub>2</sub> suspension in water as the starting material.<sup>23</sup> However, this morphology still carries the aforementioned characteristics that are detrimental to DSSC performance. Therefore, scientists have proposed many multidimensional morphologies of SnO<sub>2</sub> that have more preferred traits. Some prominent examples that have been reported in the literature include SnO<sub>2</sub> nanorods, nanoflowers, and hollow microspheres.<sup>24,25,26</sup> The focus of this project is on SnO<sub>2</sub> nanoflowers, namely its synthesis and the evaluation of its performance as semiconductor compared to SnO<sub>2</sub> spherical NPs in a DSSC.

SnO<sub>2</sub> nanoflowers (NFs) are a three-dimensional morphology of SnO<sub>2</sub> whose appearance resembles a flower. The “flower” consists of a spherical core with projecting nanorod-like “petals.” Like SnO<sub>2</sub> spherical NPs, SnO<sub>2</sub> NFs can be easily synthesized using hydrothermal methods, albeit with different starting materials.<sup>25</sup> SnO<sub>2</sub> NFs are notably larger in size and more crystalline compared to the spherical NPs. Increased size and crystallinity of the particles enhance light scattering in the DSSC, which extend the distance light travels within the cell and increase the solar conversion efficiency.<sup>27</sup> The enhanced crystallinity of SnO<sub>2</sub> NFs also decreases the chance of electrons being trap due to imperfections in crystal structure. This in turn reduces charge recombination and increase electron lifetime.<sup>8</sup> The overall expected effect is the increase in  $J_{sc}$ ,  $V_{OC}$ ,  $P_{max}$ , and  $\eta$ .

This project presents the successful synthesis of SnO<sub>2</sub> NFs using a simple hydrothermal route, and analysis of NFs-based DSSC performance. The results indicate that SnO<sub>2</sub> NFs offer

increased  $V_{OC}$  compared to spherical NPs. However,  $I_{SC}$  of the NFs-based DSSC decreases compare to that of spherical NP-based DSSC. An inspiring revelation from this project is that DSSCs made from a mixture of  $SnO_2$  NFs and spherical NPs possess higher  $V_{OC}$  and  $I_{SC}$  than those of DSSC made solely with NFs or NPs.

## EXPERIMENTAL

The procedure for synthesizing  $SnO_2$  nanospheres was adapted from Chappel et al.<sup>23</sup> The procedure for synthesizing  $SnO_2$  nanoflower particles was adapted from Qi et al.,<sup>25</sup> with some modification based on the availability of chemical reagents in the laboratory. Chemical reagents used in the experiment included  $SnO_2$  colloid (15% in water), tin(IV) chloride pentahydrate ( $SnCl_4 \cdot 5H_2O$ ), trisodium citrate dihydrate ( $Na_3C_6H_5O_7 \cdot 2H_2O$ ), sodium hydroxide (NaOH), acetic acid ( $CH_3COOH$ ), polyethylene glycol (PEG) with molecular weight of 20,000, polyethylene oxide (PEO) with molecular weight of 100,000, iodine ( $I_2$ ), lithium iodide (LiI), guanidine thiocyanate (GuSCN), 1,3-dimethylimidazolium iodine ( $C_5H_9IN_2$ ), 4-*tert*-butylpyridine ( $C_9H_{13}N$ ), N719 ruthenium complex dye, hexachloroplatinic acid ( $H_2PtCl_6$ ) and titanium(IV) chloride ( $TiCl_4$ ). Figure 3 shows the chemical structure of the N719 dye (also known as Ru535-bisTBA). Chemical solvents used in the experiment included ultrapure water, ethanol, acetonitrile, and valeronitrile.

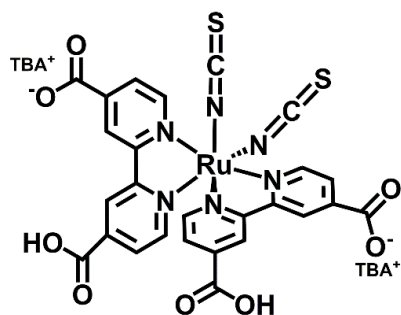


**Figure 3.** Chemical structure of N719 dye used in this experiment to fabricate DSSCs

Scanning electron microscopy (SEM) images of samples were taken using a JEOL JSM-7100F scanning electron microscope. Transmission electron microscopy (TEM) images and energy-dispersive x-ray spectra (EDS) of the samples were taken using a JEOL JEM-2100 transmission electron microscope. UV-Vis spectra were obtained using Agilent Cary 60 spectrophotometers. Photovoltaic performance were carried out using Sciencetech TLS-72-X300 as solar simulator. All chemicals were purchased from Sigma-Aldrich, Alfa Aesar, and Beantown Chemical.

#### *SnO<sub>2</sub> nanosphere synthesis.*

Glacial acetic acid (1 mL) was introduced to 30 mL of SnO<sub>2</sub> colloid (15% in water) in a round-bottom flask. The mixture was mixed for 24 hours at room temperature, and then underwent hydrothermal treatment (240 °C, 60 hours) in an autoclave reactor (Parr Instruments). The resulting solution and precipitates were mixed again to form a uniform viscous solution. This solution was characterized with TEM and EDS. PEG (MW 20,000) and PEO (MW 100,000) (2.5% wt each) were added to mixture to make the paste.

#### *SnO<sub>2</sub> nanoflower synthesis.*

SnCl<sub>4</sub>.5H<sub>2</sub>O (1 mmol) was dissolved in a solution of 15 mL ethanol, 15 mL water, and 10 mmol of NaOH. 0.3 mmol Na<sub>3</sub>C<sub>6</sub>H<sub>5</sub>O<sub>7</sub>.2H<sub>2</sub>O was then added to the solution. The mixture was then sonicated thoroughly, moved to an autoclave reactor, and treated at 200°C for 24 hours. The resulting precipitate was then washed under centrifugation twice with water and then twice with ethanol. The solid was retrieved by drying in the oven for 24 hours at 110 °C, and then weighed using an analytical balance. This solid was characterized with SEM, TEM, and EDS. Subsequently, the solid was resuspended in ethanol. PEG and PEO (2.5% wt each) were added to the mixture to make the paste.

### *Preparation of mixed nanosphere and nanoflower paste.*

Two solutions of nanoflowers and nanospheres (without PEG and PEO) were mixed in a two-to-one ratio (flowers:spheres = 2:1) based on the moles of the SnO<sub>2</sub>. This mixture is called FS21. PEG and PEO (2.5% wt each) were added to the mixture, and the mixture were then stirred thoroughly.

### *Solar cells fabrication and evaluation.*

The SnO<sub>2</sub> paste was spread on the conducting side of FTO glass evenly using the method of doctor blading, and these pieces of glass were heated to 450 °C for 30 minutes. The pieces of glass with the SnO<sub>2</sub> layer on it was then soaked in a solution of N719 dye (300 μM in ethanol) for 24 hours to make the photoanode. The counter electrode was made by depositing platinum on another piece of FTO glass. In this procedure, 15 μL of 0.01 M hexachloroplatinic acid solution is spread on the conducting side of the FTO glass using a pipette. These pieces of glass were then heated to 450 °C for 30 minutes. Two holes were drilled on the counter electrode for introduction of the electrolyte. The photoanode and the counter electrode were then sealed together by gaskets made from hot-melt film, and the electrolyte solution (0.03 M iodine, 0.05 M lithium iodide, 1.0 M 1,3-dimethylimidazolium iodine, 0.1 M 4-*tert*-butylpyridine, and 0.1 M guanidine thiocyanate, dissolved in a 1:1 solution of acetonitrile and valeronitrile) was introduced through the drilled holes. TiO<sub>2</sub>-based DSSCs were also prepared with the already available TiO<sub>2</sub> paste using the same method laid out above.

The resulting dye-sensitized solar cell was irradiated by artificial sunlight, and its generated voltage and current were measured by a multimeter. Two types of photovoltaic experiment performed were a voltage sweep experiment and a light on-off experiment.

### *Introduction of SnO<sub>2</sub> blocking layer.*

The compact SnO<sub>2</sub> blocking layer was introduced in an attempt to improve the solar cell performance. Before the SnO<sub>2</sub> particles were deposited on the FTO glass, the glass surface was treated with the SnO<sub>2</sub> colloid in water. The SnO<sub>2</sub> colloid was pipetted on the surface of the FTO glass substrates, and then the glass substrates underwent spin coating (RPM = 1000, 45 seconds) so a uniform, thin, and transparent layer of SnO<sub>2</sub> was deposited on the glass surface. These pre-treated glass substrates then went through sintering at 450 °C for 30 minutes.

*Titanium oxide coating procedure.*

Some of the photoanode with SnO<sub>2</sub> (both NPs and NFs) were coated with a layer of titanium oxide. The photoanodes were soaked in a solution of TiCl<sub>4</sub> (0.1 M) for three hours. Then the electrodes were gently rinsed with DI water, dried, and then sintered at 450 °C for 30 minutes. The resulting photoanodes were then used to fabricate solar cells, and their photovoltaic performance was checked using the same method as described in the previous section.

## **RESULTS**

### **SEM images of SnO<sub>2</sub> nanoflowers.**

SEM images for SnO<sub>2</sub> NFs are shown in Figure 4. The synthesis procedure yields SnO<sub>2</sub> NFs with the desired morphology that is comparable with results reported in literature.<sup>25</sup> The obtained SnO<sub>2</sub> NFs have similar size and shape compared to the NFs reported from Qi et al using a similar procedure. Most particles consist of many rods protruding from a center and take a flower-like shape. The particles also have diameters from 0.5 μm to 1.2 μm, indicating that they are considerably larger than the traditional SnO<sub>2</sub> NPs, whose diameters are typically between 10 nm to 50 nm.

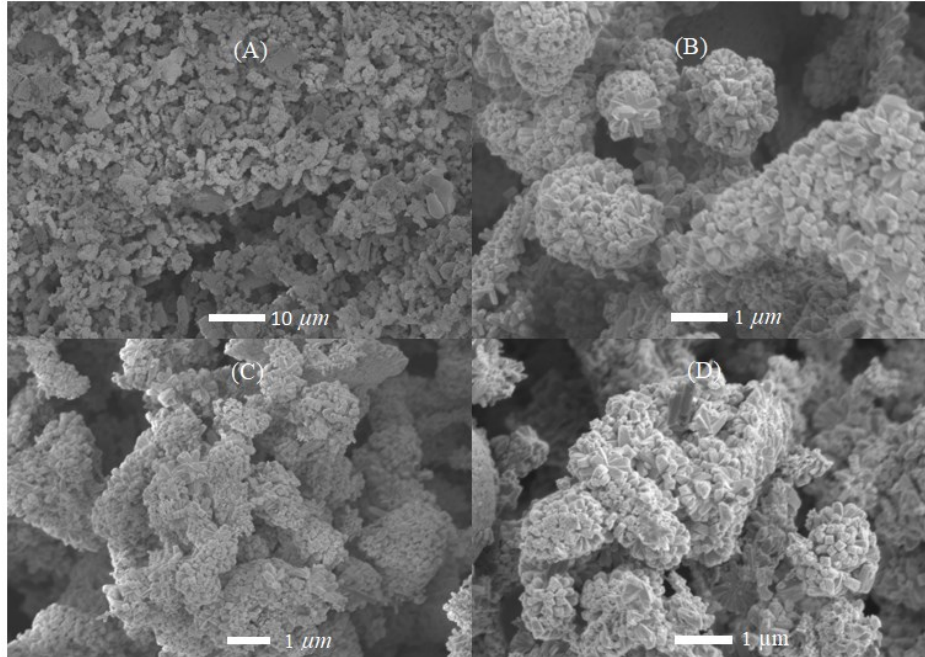


**Figure 4.** SEM images of SnO<sub>2</sub> NFs at different magnification. (A) has a scale bar with a length of 10 μm, and (B), (C), and (D) has a white scale bar with a length of 1 μm.

**TEM images and EDS analysis of SnO<sub>2</sub> spherical particles and flower-like particles.**

TEM images of SnO<sub>2</sub> NPs and NFs are shown in Figure 5. The SnO<sub>2</sub> NPs are 15 nm to 25 nm in diameter whereas the SnO<sub>2</sub> NFs are 0.5 μm to 1.2 μm in diameter. The EDS graphs of SnO<sub>2</sub> NPs and SnO<sub>2</sub> NFs are shown in Figure 6. Table 1 shows the weight composition and atomic composition of the elements from samples of each particle types.

**Table 1:** Atomic and weight composition of SnO<sub>2</sub> NPs and NFs from EDS analysis.

Sample	Element	Atomic composition (%)	Weight composition (%)
SnO <sub>2</sub> NPs	Sn	40.09	83.23
	O	59.91	16.77
SnO <sub>2</sub> NFs	Sn	45.25	85.97
	O	54.75	14.03

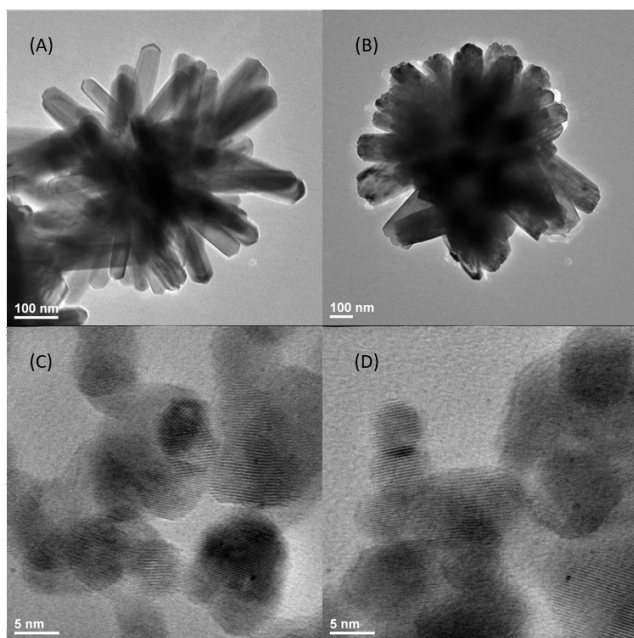


**Figure 5.** TEM images of SnO<sub>2</sub> NFs and NPs at different magnification. (A) and (B) show TEM images of SnO<sub>2</sub> NFs with a white scale bar of 100 nm. (C) and (D) show TEM images of SnO<sub>2</sub> NPs with a white scale bar of 5 nm.

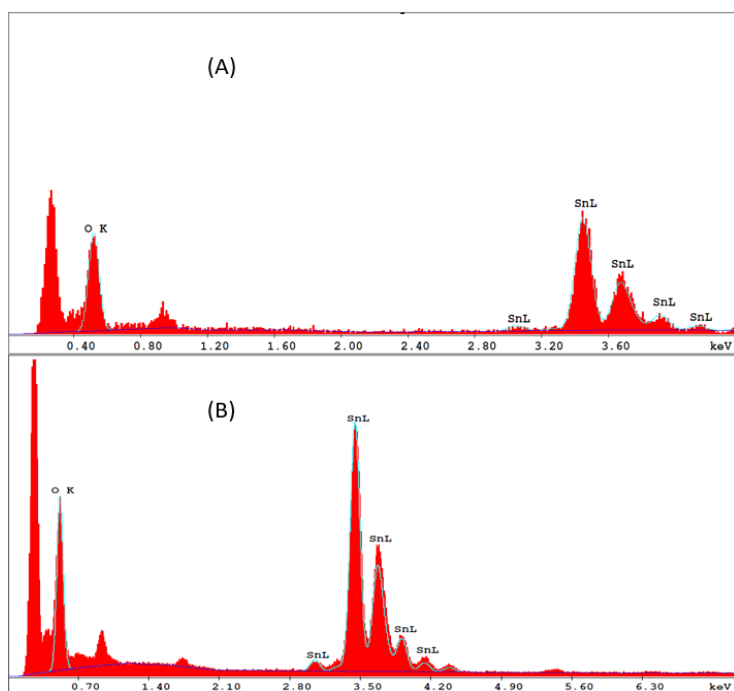


**Figure 6.** EDS spectra of SnO<sub>2</sub> NPs (A) and SnO<sub>2</sub> NFs (B).

### Visual inspection of photoanodes.

Photo images of the different types of photoanodes used in this study are shown in Figure 7. The photoanodes using SnO<sub>2</sub> NPs and TiO<sub>2</sub> NPs, shown prior to dye loading, were transparent and mostly uniform. Photoanodes using SnO<sub>2</sub> NFs have a cloudy film layer, and clumps of particles were visible, indicating that the particles were not dissolved well in the paste. Photoanodes using SnO<sub>2</sub> FS21 also had a cloudy film layer but are much more uniform and there were no visible clumps of particles.

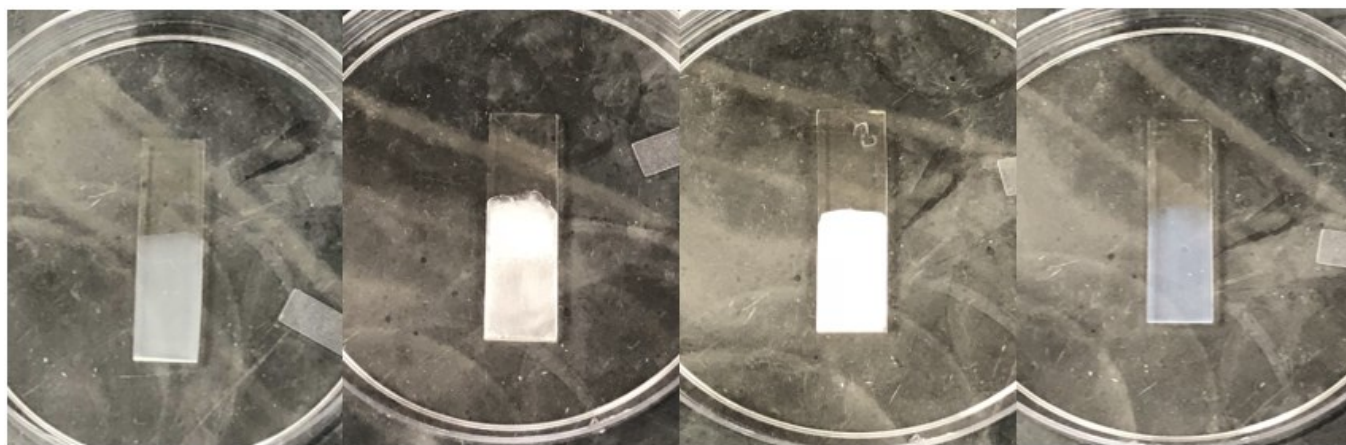


**Figure 7.** Images of photoanodes using different semiconducting materials. From left to right: SnO<sub>2</sub> NPs, SnO<sub>2</sub> NFs, SnO<sub>2</sub> FS21, and TiO<sub>2</sub> NPs.

### UV-Visible spectra of photoanodes.

UV-Vis spectra of undyed and dyed photoanodes made from different semiconducting materials are shown in Figure 8.

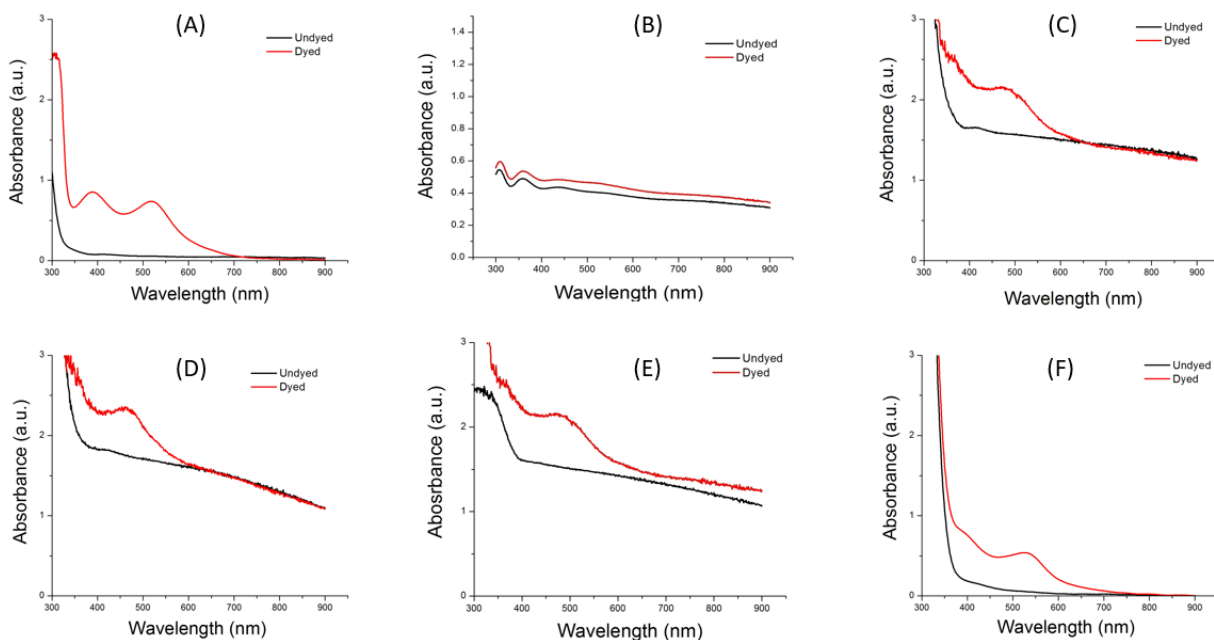


**Figure 8.** UV-Vis spectra of undyed and dyed DSSC photoanodes made from SnO<sub>2</sub> spherical particles (A), SnO<sub>2</sub> nanoflower particles (B), SnO<sub>2</sub> FS21 mixture (C), SnO<sub>2</sub> FS21 mixture with a pre-treated blocking layer of SnO<sub>2</sub> (D), FS21 with a pre-treated blocking layer of SnO<sub>2</sub> and post-treated with the titanium core shell (E), and TiO<sub>2</sub> spherical particles (F).

### DSSC Photovoltaic performance.

Figure 9 shows the representative J-V curves of DSSCs constructed using different semiconducting materials. Table 2 shows the average values for the open-circuit voltage, short-circuit current, maximum power, fill factor, and solar conversion efficiency of each type of DSSCs, with standard deviations. Figure 10 shows the representative J-T plots of DSSCs using different semiconducting materials. Each light-off period and each light-on period last twenty seconds, with five illumination periods shown.

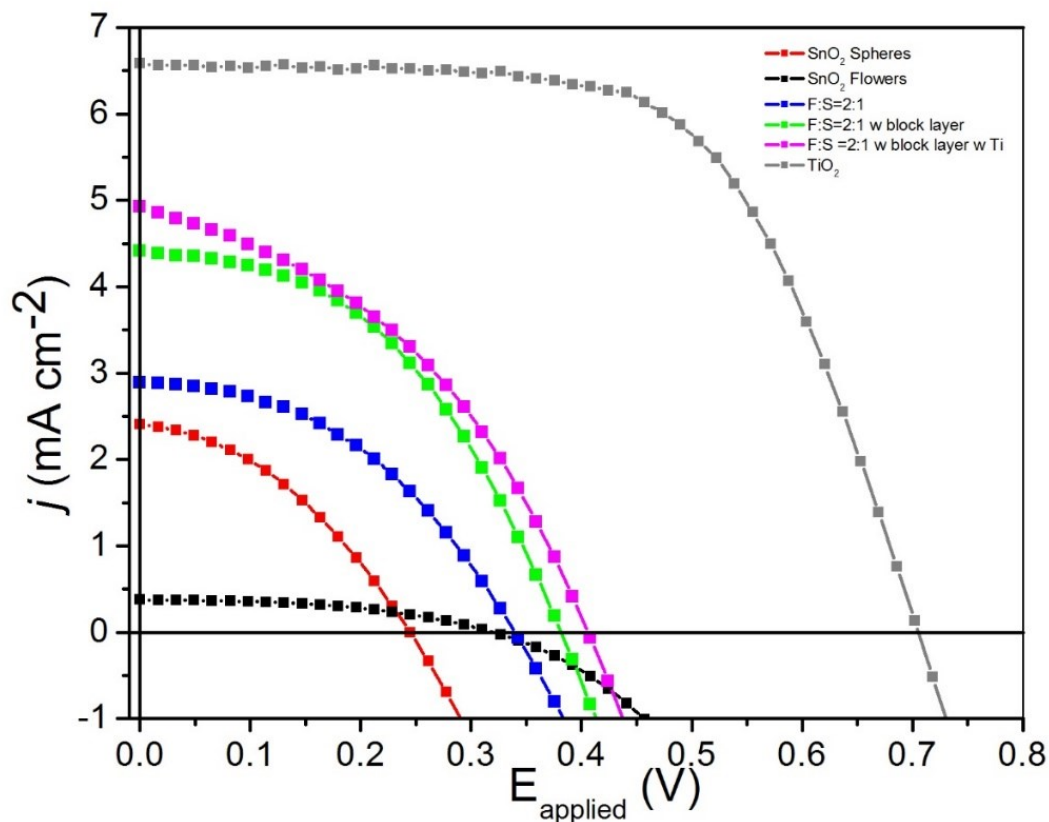


**Figure 9.** Representative J-V curves of DSSC using SnO<sub>2</sub> NPs (red), SnO<sub>2</sub> NFs (black), and FS21 (blue) as semiconductor. Also shown are J-V curves of DSSCs using the FS21 semiconductor film with modifications applied to the photoanode, namely the introduction of an SnO<sub>2</sub> blocking layer (green), and the introduction of both an SnO<sub>2</sub> blocking layer and a TiO<sub>2</sub> surface coating layer (magenta). A J-V curve of a DSSC using TiO<sub>2</sub> NPs (gray) is included for comparison.

**Table 2:** Average values of open-circuit voltage, short-circuit current, maximum power, fill factor, and solar conversion efficiency of different types of DSSCs, with standard deviations.

Samples	$I_{SC}$ (mA cm <sup>-2</sup> )	$V_{OC}$ (V)	$P_{max}$ (mW cm <sup>-2</sup> )	FF (%)	$\eta$ (%)
NPs	$2.45 \pm 0.05$	$0.26 \pm 0.02$	$0.24 \pm 0.02$	$37.8 \pm 0.4$	$0.27 \pm 0.02$
NFs	$0.39 \pm 0.07$	$0.34 \pm 0.02$	$0.06 \pm 0.01$	$48 \pm 2$	$0.07 \pm 0.01$
FS21	$2.5 \pm 0.2$	$0.344 \pm 0.007$	$0.38 \pm 0.02$	$45 \pm 1$	$0.44 \pm 0.02$
FS21 with block layer	$3.8 \pm 0.6$	$0.384 \pm 0.002$	$0.66 \pm 0.09$	$45 \pm 2$	$0.75 \pm 0.09$
FS21 with block layer and TiCl <sub>4</sub> treatment	$4.9 \pm 0.2$	$0.41 \pm 0.02$	$0.80 \pm 0.08$	$39 \pm 1$	$0.91 \pm 0.09$
TiO <sub>2</sub>	$6.7 \pm 0.3$	$0.69 \pm 0.01$	$2.75 \pm 0.09$	$60 \pm 2$	$3.1 \pm 0.1$

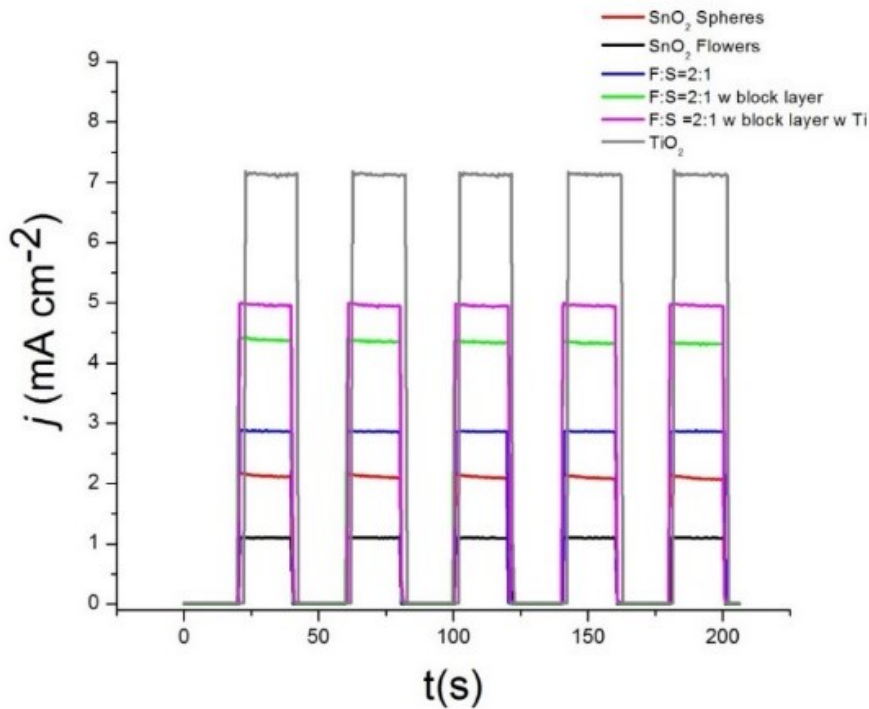


**Figure 10.** Representative J-T plots of DSSCs using SnO<sub>2</sub> NPs (red), SnO<sub>2</sub> NFs (black), and FS21(blue) as the semiconductors, with J-T graphs of DSSC using the FS21 mixture with an SnO<sub>2</sub>

blocking layer (green), and the introduction of both an SnO<sub>2</sub> blocking layer and a TiO<sub>2</sub> surface coating layer (magenta). J-T graph of DSSC using TiO<sub>2</sub> NPs (gray) is also included for comparison. Each light-off period and each light-on period last twenty seconds.

## DISCUSSION

### Characteristics of SnO<sub>2</sub> particle.

SnO<sub>2</sub> NPs and NFs were imaged using SEM and TEM and also underwent EDS analysis. Images of SnO<sub>2</sub> NPs and NFs indicate that the particles synthesized in this experiment possess similar size and shape compared to those reported in the literature.<sup>23,25</sup> SnO<sub>2</sub> NPs reported in Chappel et al have diameter of 18 nm to 27 nm, whereas the NPs from this study have a diameter of 15 nm to 25 nm. SnO<sub>2</sub> NFs reported in Qi et al are 0.6 μm to 1.5 μm in diameter, while the NFs synthesized from this experiment are 0.5 μm to 1.2 μm in diameter. The morphology of SnO<sub>2</sub> NPs reported in this study is spherical with fine surface, which is comparable to the morphology of NPs reported in Chappel et al. Furthermore, both the shapes of SnO<sub>2</sub> NFs reported in this study and in Qi et al are also similar. The nanoflower particles from both sources take a flower-like shape, with nanorods protruding from the center of the particles. Both the size and morphologies of synthesized NPs and NFs in this study are similar to what was expected from the adopted procedure and are suitable for further experiments.

The EDS spectra of SnO<sub>2</sub> NPs and NFs are shown in Figure 6. As expected, two major elements, Sn and O, are present in the spectra. However, the atomic composition of the samples obtained from EDS does not exactly match what is expected. For SnO<sub>2</sub> samples, the anticipated atomic ratio of Sn to O should be 1 to 2. However, as indicated in Table 1, the atomic ratios of Sn to O are 2 to 3 in SnO<sub>2</sub> NP samples and about 4 to 5 in SnO<sub>2</sub> NF samples. A possible explanation for this deviation is that under the operating condition of TEM and EDS (high energy x-ray and

under vacuum), oxygen migration can happen, and the result is that the sample looks oxygen-poor. Therefore, in this study, EDS analysis is mainly used only to the extent of confirming the presence of Sn and O in the sample.

### **Photoanode characteristics.**

The photoanodes of the DSSCs were characterized by visual inspection, UV-Visible spectroscopy, TEM, EDS, and SEM. As shown in Figure 7, photoanodes made with SnO<sub>2</sub> NPs and TiO<sub>2</sub> NPs have a uniform and transparent film layer, whereas photoanodes made of SnO<sub>2</sub> NFs show particular irregularity in the film layer, with many clumps of particles visible to the naked eye. Photoanodes made with SnO<sub>2</sub> FS21 have a much more uniform appearance than those made of SnO<sub>2</sub> NFs, but they have a more cloudy appearance compared to NP or TiO<sub>2</sub> films. The main reason for these disparities in appearance is the difference in the dispersiveness of the particles in different solvents, namely water and ethanol. SnO<sub>2</sub> and TiO<sub>2</sub> NPs, though not entirely soluble in water, could form colloids, which is proven from past literature,<sup>28</sup> and this allows the paste to be spread evenly on the surface of FTO glass by doctorblading.

The larger SnO<sub>2</sub> NFs, typically 1 μm in diameter, do not form a colloidal suspension in water, leading to clump or uneven films after doctorblading. Therefore, the approach taken in this study was to create a suspension of SnO<sub>2</sub> NFs in a solvent that was kept constantly under stirring. Furthermore, on a FTO glass surface that is not perfectly clean, the water-based suspension could not be spread out evenly because water has a high surface tension and tends to form droplets. Therefore, ethanol was employed as the solvent for the SnO<sub>2</sub> NFs suspension, and the substitution did help with the doctorblading process. However, since this suspension is not a proper colloid, the thin film made from it on the photoanode is opaque, and clumps of particles are visible.

The mixture of SnO<sub>2</sub> NPs and NFs, referred to in this paper as FS21, produced thin films on photoanode that possess some of the characteristics of that of NPs with some of the characteristics of that of NFs, based on visual inspection. The deposited layers are much more uniform than those made from the SnO<sub>2</sub> NFs paste, and these films from FS21 have a uniformity that is comparable to that of the SnO<sub>2</sub> NPs films. This might be because the SnO<sub>2</sub> NPs colloid component in the mixture provides the viscosity needed for the paste to be spread evenly on the FTO glass surface. The SnO<sub>2</sub> NFs component of the mixture is responsible for the opacity of the film as the nanoflower particles are only suspended in the mixture without forming colloid.

UV-Visible spectroscopy was employed to investigate the materials deposited on the photoanode more thoroughly. By examining the UV-Vis spectra of each photoanode, this study could draw some conclusions about how the SnO<sub>2</sub> are deposited on the glass surface. Figure 8 shows all of the UV-Vis spectra of photoanodes made from different semiconducting materials. From these spectra, it is clear that the different materials show different absorption patterns that could be used to determine whether the materials are deposited successfully on the glass surface and whether the amount of materials deposited are desirable. The spectrum obtained from the undyed photoanode made from SnO<sub>2</sub> NPs is mostly flat in the visible region, and the absorbance is relatively low. The major peak from this spectrum occurs at 330-340 nm, which is similar to the expected range of 325-350 nm for SnO<sub>2</sub> particles.<sup>29</sup> This indicates that the SnO<sub>2</sub> particles were properly deposited on the FTO glass surface. The spectrum for photoanodes based on SnO<sub>2</sub> NFs, however, only show a low-absorbance peak in the same range. This indicates that the particles are indeed SnO<sub>2</sub>, but the relative concentration compared to NP-based photoanodes is much lower. The main reason for this low absorbance is the inability of SnO<sub>2</sub> NFs to form colloids. Therefore, when deposited by doctorblading, the nanoflower particles could not be spread evenly on the

surface, creating visible clumps as mentioned before, as well as leaving gaps on the glass surface. Therefore, more light from the UV-vis source was transmitted through, and the absorbance is lower.

The photoanode made from FS21 shows different behaviors in its UV-vis spectrum. Contrary to NPs-based photoanode, the photoanode made from the mixture does not show near-zero absorbance in the visible and near-infrared range. Instead, it shows absorbance of around 1.5 absorbance units, and the absorbance value in this range increases slightly from the near-infrared to the high-energy end of the visible spectrum (from 900 nm to 400 nm as show in the spectrum in Figure 8). The high absorbance from the film in this range is consistent with the opacity of the film seen in Figure 7. Compared to that made from SnO<sub>2</sub> NPs, it scatters more light, and thus much less light can pass directly through the film to reach the detector. Furthermore, the gradual increase in absorbance over the range is indicative of scattering by particles on the photoanode. As the wavelength of the incident light gets lower, the light is more likely to be scattered as it could interact with smaller particles.<sup>30</sup> The scattered light does not reach the detector, and the instrument reads the decrease in intensity as absorbance although light is not absorbed by the SnO<sub>2</sub>. Therefore, as the wavelength of light decreases, the absorbance measurement increases. The UV-vis spectrum of FS21-based photoanode shows a peak at 375 nm, which is more redshifted than the characteristic absorption range of 325-350 nm for SnO<sub>2</sub>. A possible reason for this redshift is the unique nanostructure of the particles, and the phenomenon has been reported elsewhere.<sup>31</sup> UV-vis spectrum of photoanodes made from FS21 with a blocking layer shows similar features to the spectrum of a similar photoanode without this blocking layer. This is plausible due to the fact that the blocking layer is made from SnO<sub>2</sub> colloid in water, and its normal absorption at 325 nm is masked by the stronger signal from the film.

The spectrum of the photoanode made of TiO<sub>2</sub> NPs for reference shows similar features of that made of SnO<sub>2</sub> NPs in the near-infrared and visible range. The deposited TiO<sub>2</sub> film is transparent and gives near-zero absorbance in the 900-400 nm range. The spectrum shows a major peak at 400 nm, which is consistent with the normal value expected for TiO<sub>2</sub>.<sup>32</sup> This result is consistent with the characteristics of TiO<sub>2</sub> and SnO<sub>2</sub>. TiO<sub>2</sub> absorbs photon at lower energy compared to SnO<sub>2</sub> because it has a smaller band gap (3.2 eV compared to 3.8 eV).<sup>33</sup> The UV-vis spectrum of the photoanode made of FS21 with a blocking layer and a TiO<sub>2</sub> coating shows similar features of that made from just the FS21 without any modification in the near-infrared and the visible range. One distinction for the former is that the major peak of this spectrum starts at 400 nm. This indicates that the TiO<sub>2</sub> was successfully deposited on the SnO<sub>2</sub> film, hence the redshift in absorbance.

Figure 8 also shows the spectra of dyed photoanodes, and in every type of photoanode, the adsorbed dye on the surface create a clear distinction in UV-vis spectra compared to that of undyed ones. A major difference is the addition of two major peaks within the visible range, at 400 nm and 540 nm, which is at the blue and green spectral regions, respectively. This characteristic in the spectra confirms the successful adsorption of N719 dye on the semiconductor surface as the features are also consistent with the absorbance spectrum of this dye.<sup>34</sup> Also, these two absorption peaks are in accordance with the dark red color of dyed photoanodes. Because the dye absorbs blue and green light, the photoanode shows the dark red color from unabsorbed photons. For the SnO<sub>2</sub> NPs-based photoanode, these two major peaks from the dye are prominent, as there is no other absorption occurring in this range. Other types of photoanodes, as mentioned earlier, have absorption occurring at or around 400 nm. Therefore, instead of two clear peaks, the spectra of these photoanodes present a distinct peak at 540 nm and a shoulder at 400 nm. An exception is the

spectrum of the SnO<sub>2</sub> NFs-based photoanode, which does not clearly show this feature from the dye. A possible explanation is that the dye is not adsorbed well on the surface of the nanoflower particles; therefore, the concentration of dye on the photoanode is very low, and no prominent feature could be detected. This explanation is supported by visual inspection, as dyed photoanodes made from SnO<sub>2</sub> NFs only have a faint red color.

### **Photovoltaic performance of dye-sensitized solar cell.**

The photovoltaic performance of the fabricated DSSCs is examined mainly through analysis of J-V curves and J-T graphs. From J-V curves, most of the important parameters of a photovoltaic experiment can be obtained and calculated, such as open-circuit voltage, short-circuit current, fill factor, maximum power, and solar cell efficiency. By evaluating these parameters both separately and holistically, this study determines which type of SnO<sub>2</sub>-based solar cells have the best performance, how this performance compares to the results already reported in the literature, and possible future approaches for improving the performance of these solar cells.

Overall, the most obvious trait of SnO<sub>2</sub>-based DSSCs is that their performance is inferior compared to that of DSSCs made from TiO<sub>2</sub>. This is an expected result as TiO<sub>2</sub> is still considered the most optimal material for DSSC fabrication. However, as shown in Figure 9 and Table 2, among SnO<sub>2</sub>-based DSSCs, there is improvement in performance when extra modifications are applied to the solar cells. Although the best-performing SnO<sub>2</sub>-based DSSCs from this study could not quite reach the quality and performance of a TiO<sub>2</sub>-based DSSC, this positive trend provides a promising approach to investigate and modify SnO<sub>2</sub> films so that they could produce better photovoltaic performance.

According to Figure 9 and Table 2, DSSCs based solely on SnO<sub>2</sub> NPs and DSSCs based solely on SnO<sub>2</sub> NFs have very distinct characteristics in their photovoltaic performance. NP-based

DSSCs produce a short circuit current of  $2.45 \text{ mA cm}^{-2}$ , which is much higher than that of NF-based DSSCs ( $0.39 \text{ mA cm}^{-2}$ ). However, the open-circuit voltage of NF-based DSSCs is  $0.34 \text{ V}$ , which is a considerable improvement compared to a voltage of  $0.26 \text{ V}$  of NP-based DSSCs. The  $J_{\text{SC}}$  and  $V_{\text{OC}}$  of NP-based is slightly lower than the reported values in the literature ( $3.0 \text{ mA cm}^{-2}$  in  $J_{\text{SC}}$ ,  $0.32 \text{ V}$  in  $V_{\text{OC}}$ ).<sup>35</sup> A possible reason for this slightly inferior performance can be the difference in fabrication techniques and in conditions in different laboratory environments that lead to difference in the thickness of the film and the quality of the cells. However, the discrepancy is not too severe to affect the conclusion of this study. For NF-based DSSCs, the main reason for its low  $J_{\text{SC}}$  is its inability to adsorb the dye on its surface, as mentioned earlier. Without a uniform, concentrated dye layer, the cell could not generate many electrons from sunlight, and the produced current, as a result, is very low. The interesting feature of NF-based DSSCs lies in its considerably higher  $V_{\text{OC}}$  compared to NP-based DSSCs. This improvement likely results from the flower-like nanostructure of the particles. Being much more crystalline than NPs, these NFs do not have as many surface defects in their crystal structures.<sup>25</sup> These defects are the primary sites that trap electrons and allow charge recombination. The  $\text{SnO}_2$  NFs interface limits this phenomenon and provides better electron directionality and more efficient charge transfer, which result in a better  $V_{\text{OC}}$ . However, because its  $J_{\text{SC}}$  is too low, NF-based DSSCs have an inferior  $P_{\text{max}}$  and  $\eta$  ( $0.06 \text{ mW cm}^{-2}$  and  $0.07\%$ ) compared to that of NP-based DSSC ( $0.24 \text{ mW cm}^{-2}$  and  $0.27\%$ ). Nevertheless, with a better  $V_{\text{OC}}$  as well as a better FF ( $48\%$  compared to  $37.8\%$ ),  $\text{SnO}_2$  NFs clearly show their potential for use in DSSCs.

Each individual type of particle possesses a desired advantage over the other, but it also has a drawback that needs to be improved. If both  $J_{\text{SC}}$  and  $V_{\text{OC}}$  could be optimized, the photovoltaic performance of the solar cell should be higher. The approach this study takes is to make a mixture

of these two morphologies and apply it to make the DSSC semiconductor film. From Figure 9 and Table 2, it is clear that the DSSCs made with FS21 demonstrate better overall performance than DSSCs made with films of the individual types of particle. All photovoltaic parameters of FS21-based DSSCs, except for FF, are superior than those of the NP-based and NF-based ones. By mixing these two SnO<sub>2</sub> particle types together, their advantages are promoted whereas their weaknesses are suppressed. The J<sub>SC</sub> of FS21-based cell is similar to that of NP-based cells (2.5 mA cm<sup>-2</sup> to 2.45 mA cm<sup>-2</sup>), and the V<sub>OC</sub> of FS21-based cell is similar to that of NF-based cells (0.344 V to 0.34 V). Introducing the nanoflower particles into the colloid of spherical particles allows the nanoflowers to be deposited evenly on the glass surface, and the dye is also able to adsorb more visible light. Thus, the photocurrent generated by these cells is much improved. The mixture also exhibits the higher voltage from the NFs. Therefore, the overall performance of the FS21-based cells is higher than that of NP-based cells (P<sub>max</sub> of 0.38 mW cm<sup>-2</sup> compared to 0.24 mW cm<sup>-2</sup>; η of 0.44 % compared to 0.27 %).

The introduction of a blocking layer made from SnO<sub>2</sub> colloidal solution in water further enhanced the performance of the DSSCs. Compared to FS21-based cells without this modification, solar cells made from FS21 with the blocking layer show superior J<sub>SC</sub> (3.8 mA cm<sup>-2</sup> to 2.5 mA cm<sup>-2</sup>), V<sub>OC</sub> (0.384 V to 0.344 V), P<sub>max</sub> (0.66 mW cm<sup>-2</sup> to 0.38 mW cm<sup>-2</sup>), and η (0.75% to 0.44%). The values for the fill factor of each type of DSSC remain the same (45%). These improved values prove that the introduction of a blocking layer can enhance the photovoltaic performance of the FS21-based solar cell. This blocking layer serves two purposes for improving solar cell performance. First, this layer minimizes the effect of charge recombination, thus increasing the photocurrent and photovoltage. The semiconductor usually cannot completely cover the entire FTO surface, which would leave some regions of exposed FTO glass. Unlike the semiconducting

SnO<sub>2</sub>, which has a CB, a VB, and thus a band gap, FTO energy levels are more like a continuum. Therefore, electrons from the dye at these regions are more likely to go through recombination, as there is no band gap to prevent them from reversing their courses. These electrons are lost to solution in contact with the exposed FTO and thus do not contribute to the photocurrent. Second of all, the blocking layer prevents I<sub>3</sub><sup>-</sup> from interacting with the FTO surface. This interaction could reduce I<sub>3</sub><sup>-</sup> and create a pocket of electrons, which reduce the amount of electrons driven through the circuit. By addressing these problems, the blocking layer dramatically enhances the current and voltage produced by the DSSCs.

A second modification, the addition of the TiO<sub>2</sub> coating layer, also improves the photovoltaic performance of solar cells. FS21-based DSSCs utilizing both a blocking layer and a TiO<sub>2</sub> coating express much improved values at almost all important photovoltaic parameters compared to those without a TiO<sub>2</sub> coating, including J<sub>SC</sub> (4.9 mA cm<sup>-2</sup> to 3.8 mA cm<sup>-2</sup>), V<sub>OC</sub> (0.41 V to 0.384 V), P<sub>max</sub> (0.80 mW cm<sup>-2</sup> to 0.66 mW cm<sup>-2</sup>), and η (0.91% to 0.75%). This TiO<sub>2</sub> layer improves solar cell performance in two ways. First, it reduces charge recombination at the FTO-electrolyte interface by creating an energy barrier, thus forcing the electrons into the circuit.<sup>36</sup> Second, this TiO<sub>2</sub> layer enhance the adsorption of dye molecules to the surface. A uniform coating of TiO<sub>2</sub> presents the same surface for anchoring the dye as would a pure TiO<sub>2</sub> film. A troubling trend for the introduction of the TiO<sub>2</sub> layer is the decrease in fill factor (from 45% to 39%), indicating some aspects of the cell quality have been compromised after the TiO<sub>2</sub> deposition treatment. A cross-sectional image of a photoanode that underwent this treatment taken using SEM is shown in Figure 11.

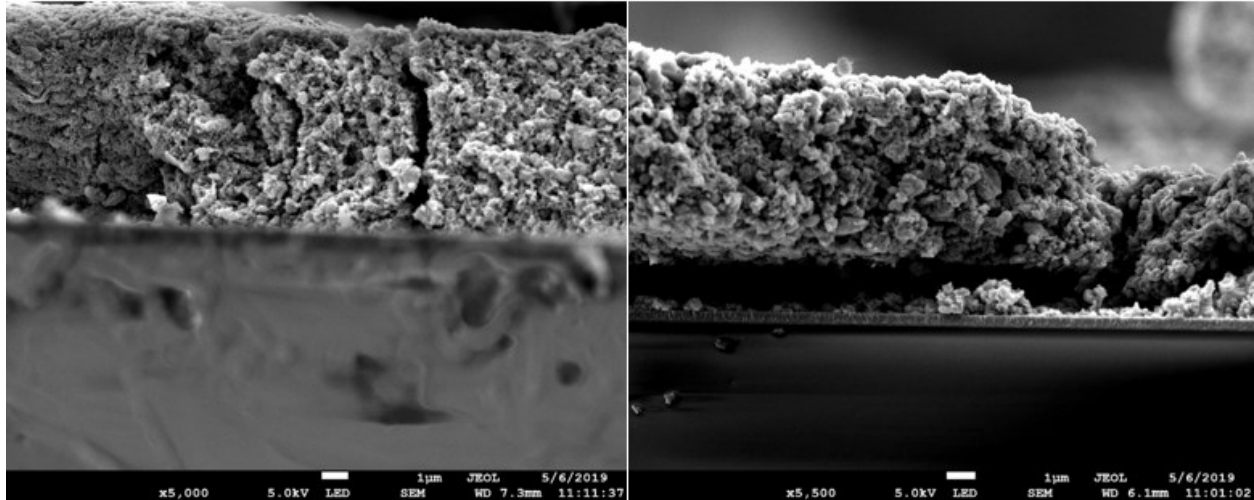


**Figure 11.** SEM cross-sectional images of FS21-based photoanodes that has not undergone  $\text{TiO}_2$  treatment (left) and has undergone  $\text{TiO}_2$  treatment (right).

Examination of these cross-sectional images show that the photoanode that went through the  $\text{TiO}_2$  deposition treatment shows a distinctive feature at the  $\text{SnO}_2$  film – FTO glass interface. The  $\text{SnO}_2$  film in this photoanode looks like it is lifted up away from the FTO surface, creating a considerable gap between the two. This feature is not present at the photoanode that does not go through  $\text{TiO}_2$  deposition treatment. This same phenomenon was observed in other samples. Therefore, it is likely that the gap was caused by the  $\text{TiO}_2$  treatment. The presence of this gap compromises the ability of electrons to move from the  $\text{SnO}_2$  to the FTO surfaces, likely introducing a considerable resistance in the cells. This would explain the decrease in fill factor for these samples. The emergence of this feature likely comes from the usage of  $\text{TiCl}_4$  - the precursor of  $\text{TiO}_2$  in this treatment, and a highly reactive reagent itself. The severity of this damage to the surface apparently correlates with the amount of time the photoanode is soaked in the  $\text{TiCl}_4$  solution. Even though this feature arises after three hours of soaking, the semiconducting layer remains adhered to the FTO glass. However, soaking the photoanodes in the solution for any period

of time longer than 5 hours causes the SnO<sub>2</sub> layer to start flaking off from the glass surface. Therefore, for future work, a more benign method to deposit TiO<sub>2</sub> on the SnO<sub>2</sub> layer should be developed. However, the TiO<sub>2</sub> layer clearly improve the overall photovoltaic performance of the DSSCs.

The J-T graphs of the DSSCs shown in Figure 10 demonstrate how the solar cells respond to light by producing photocurrent. Each “off” period last 20 seconds, and each “on” period also last 20 seconds. From Figure 10, it is clear that all six types of DSSCs show a photocurrent response. The magnitude of the photocurrent is consistent with the results obtained from the J-V curve. The SnO<sub>2</sub> NF-based DSSC produces the least current, followed by the SnO<sub>2</sub> NP-based DSSC and the FS21-based DSSC. DSSC made from FS21 with an addition of a blocking layer has improved photocurrent compared to the one without, and the introduction of the TiO<sub>2</sub> layer further enhances the photocurrent of the cell. As expected, the TiO<sub>2</sub>-based DSSCs produce the most photocurrent under the same condition.

## **CONCLUSION**

In this study, an innovative morphology of SnO<sub>2</sub>, the flower-like nanoparticles, was synthesized and applied to the fabrication of dye-sensitized solar cells. The particles themselves are difficult to deposit on the FTO glass surface to create photoanodes. Therefore, their solar cell performance are inferior compared to solar cells made from the more traditional SnO<sub>2</sub> spherical nanoparticles. However, nanoflowers provide some upsides that could be exploited, such as higher open-circuit voltage and fill factor. The approach used here to optimize the advantages of both the spherical particles and flower-like particles is to create of mixture of these two types and to use this mixture to fabricate dye-sensitized solar cells. The result is that the performance of DSSCs based on the mixture is much improved compared to those made of just a single particle type. This

result presents the potential use of SnO<sub>2</sub> nanoflowers in fabricating DSSCs and perhaps replacing or complementing the more widely used TiO<sub>2</sub> as semiconductor.

This study also introduces two modifications to the photoanode to further enhance photovoltaic performance. The first is the addition of a blocking layer between the FTO glass – SnO<sub>2</sub> layer interface. The second modification is the incorporation of a thin TiO<sub>2</sub> layer on the SnO<sub>2</sub> layer through solution-based deposition. Both of these methods, as shown from the experimental results, indeed improve the photovoltaic performance of the DSSCs. However, for the deposition of a TiO<sub>2</sub> layer, a less invasive method should be developed to replace the use of TiCl<sub>4</sub> because this method damages the SnO<sub>2</sub> film.

Overall, this study demonstrates that SnO<sub>2</sub>-based DSSCs, although still inferior compared to DSSCs made from TiO<sub>2</sub>, do have the potential to match TiO<sub>2</sub> in terms of performance. Utilizing a novel three-dimensional nanostructure, core-shell construction, and other innovative modification for the cells, scientists have reported a performance of as high as 4.3% in solar conversion efficiency, 18 mA cm<sup>-2</sup> in short-circuit current, and 0.51 V in open-circuit voltage.<sup>37</sup> Most studies investigating the performance of SnO<sub>2</sub>-based DSSCs reported a range of values from 0.5% to 3% for solar conversion efficiency.<sup>8</sup> The highest value for solar conversion efficiency observed here is 0.91% and does fall into the aforementioned range, but it indicates that there are further modifications necessary to improve the performance to that of state-of-the-art SnO<sub>2</sub> based DSSCs.

Possible future works built on the results of this study include the transition to DSSCs made with aqueous electrolyte. Although water is considered harmful for DSSC performance, as mentioned earlier, it is a preferred solvent for the electrolyte due to its accessibility, minimal risk, and environmental friendliness. Organic solvents such as acetonitrile and valeronitrile carry the

inherent risk of being highly flammable, and their combustion products are also toxic. A full transition to dye-sensitized solar cells using aqueous electrolytes is considered a final goal in this subfield.<sup>2</sup> Regarding the traditionally poor performance of DSSCs in aqueous electrolyte, many components, such as dye molecules, counter electrode materials, and electrolyte redox couples, need to be replaced by more suitable alternatives that are stable in aqueous media, and additives will be needed to enhance the interfacial interaction. Nevertheless, SnO<sub>2</sub>, especially in three-dimensional morphologies such as the NF particles represent a promising candidate for making semiconductor film for the aqueous dye-sensitized solar cells.

## REFERENCES

- (1) Ekwurzel, B.; Boneham, J.; Dalton, M. W.; Heede, R.; Mera, R. J.; Allen, M. R.; Frumhoff, P. C. The Rise in Global Atmospheric CO<sub>2</sub>, Surface Temperature, and Sea Level from Emissions Traced to Major Carbon Producers. *Climatic Change*. **2017**, *144*, 579-590.
- (2) Bella, F.; Gerbaldi, C.; Barolo, C.; Gratzel, M. Aqueous Dye-sensitized Solar Cells. *Chem. Soc. Rev.* **2015**, *44*, 3431-3473.
- (3) Sharma, S.; Jain, K. K.; Sharma, A. Solar Cells: In Research and Applications – A Review. *Mater. Sci. Appl.* **2015**, *6*, 1145-1155.
- (4) Bagher, A. M.; Vahid, M. M. A.; Mohsen, M. Types of Solar Cells and Application. *Amer. J. Opt. Photonics* **2015**, *3*, 94-113.
- (5) Chopra, K. L.; Paulson, P. D.; Dutta, V. Thin Film Solar Cells: An Overview. *Prog. Photovolt: Res. Appl.* **2004**, *12*, 69-92.
- (6) O'Regan, B.; Gratzel, M. A Low-cost, High-efficiency Solar Cell Based on Dye-sensitized Colloidal TiO<sub>2</sub> Film. *Nature*, **1991**, *353*, 737-740.
- (7) Bisquert, J. Dilemmas of Dye-sensitized Solar Cells. *ChemPhysChem*, **2011**, *12*, 1633-1636.
- (8) Wali, Q.; Fakharuddin, A.; Jose, R. Tin Oxide as a Photoanode for Dye-sensitized Solar Cells: Current Progress and Future Challenges. *J. Power Sources*, **2013**, *293*, 1039-1052.
- (9) Irvine, S. Solar Cells and Photovoltaics. In: *Springer Handbook of Electronic and Photonic Materials*; Kasap, S., Capper P., Eds; Springer: 2017; pp 1097-1109.
- (10) Macaira, J.; Andrade, L.; Mendes, A. Review on Nanostructured Photoelectrodes for Next Generation Dye-sensitized Solar Cells. *Renewable & Sustainable Energy Rev.* **2013**, *27*, 334-349.

- (11) Gong, J.; Sumathy, K.; Qiao, Q.; Zhou, Z. Review on Dye-sensitized Solar Cells (DSSCs): Advanced Techniques And Research Trends. *Renewable & Sustainable Energy Rev.* **2017**, *68*, 234-246.
- (12) Sharma, K.; Sharma, V.; Sharma, S.S. Dye-sensitized Solar Cells: Fundamentals and Current Status. *Nanoscale Res. Lett.* **2018**, *13*, 381.
- (13) Raga, S.R; Barea, E.M.; Fabregat-Santiago, F. Analysis of the Origin of Open Circuit Voltage in Dye Solar Cells. *J. Phys. Chem. Lett.* **2012**, *3*, 1629-1634.
- (14) Qi, B.; Wang, J. Fill Factor in Organic Solar Cells. *Phys. Chem. Chem. Phys.* **2013**, *15*, 8972-8982.
- (15) Park, S.; Seo, M. Chapter 5: Interface Application in Nanomaterials. In: *Interface Science and Technology*; Elsevier: 2011; pp 333-429.
- (16) Fakharuddin, A.; Ahmed, I.; Khalidin, Z.; Yusoff, M. M.; Jose, R. Channeling of Electron Transport to Improve Collection Efficiency in Mesoporous Titanium Dioxide Dye-Sensitized Solar Cell Stacks. *Appl. Phys. Lett.* **2014**, *104*, 053905.
- (17) Varghese, O. K.; Paulose, M.; Grimes, C. A. Long Vertically Aligned Titania Nanotubes on Transparent Conducting Oxide for Highly Efficient Solar Cells. *Nat. Nanotechnol.* **2009**, *4*, 592-597.
- (18) Kim, J; Zhu, K.; Yan, Y.; Perkins, C. L.; Frank, A. J. Microstructure and Pseudocapacitive Properties of Electrodes Constructed of Oriented NiO-TiO<sub>2</sub> Nanotube Arrays. *Nano Lett.* **2010**, *10*, 4099-4104.
- (19) Tiwana, P.; Docampo, P.; Johnston, M. B.; Snaith, H. J.; Herz, L. M. Electron Mobility and Injection Dynamics in Mesoporous ZnO, SnO<sub>2</sub>, and TiO<sub>2</sub> Films Used in Dye-sensitized Solar Cells. *ACS Nano* **2011**, *5*, 6, 5158-5166.

- (20) Kay, A.; Gratzel, M. Dye-sensitized Core-Shell Nanocrystals: Improved Efficiency of Mesoporous Tin Oxide Electrodes Coated with a Thin Layer of an Insulating Oxide. *Chem. Mater.* **2002**, *14*, 2930-2935.
- (21) Park, N.; Kang, M. G.; Ryu, K. S.; Kim, K. M.; Chang, S. H. Photovoltaic Characteristics of Dye-sensitized Surface-modified Nanocrystalline SnO<sub>2</sub> Solar Cells. *J. Photochem. Photobio., A* **2004**, *161*, 105-110.
- (22) Niiobe, D.; Makari, Y.; Kitamura, T.; Wada, Y.; Yanagida, S. Origin of Enhancement in Open-circuit Voltage by Adding ZnO to Nanocrystalline SnO<sub>2</sub> in Dye-sensitized Solar Cells. *J. Phys. Chem. B* **2005**, *109*, 17892-17900.
- (23) Chappel, S.; Zaban, A. Nanoporous SnO<sub>2</sub> Electrodes for Dye-sensitized Solar Cells: Improved Cell Performance by the Synthesis of 18 nm SnO<sub>2</sub> Colloids. *Sol. Energy Mater. Sol. Cells* **2000**, *71*, 141-152.
- (24) Vuong, D. D.; Hien, V. X.; Trung, K. Q.; Chien, N. D. Synthesis of SnO<sub>2</sub> Micro-spheres, Nano-rods and Nano-flowers via Simple Hydrothermal Route. *Physica E* **2011**, *44*, 345-349.
- (25) Qi, T.; Wang, Q.; Zhang, Y.; Wang, D.; Yang, R.; Zheng, W. Growth of Flower-like SnO<sub>2</sub> Crystal and Performance as Photoanode in Dye-sensitized Solar Cells. *Materials & Design* **2016**, *112*, 436-441.
- (26) Zhang, X.; Huang, M.; Qiao, Y. Synthesis of SnO<sub>2</sub> Single-layered Hollow Microspheres and Flowerlike nanospheres through a Facile Template-free Hydrothermal Method. *Mater. Lett.* **2013**, *95*, 67-69.
- (27) Zhang, Y.; Myers, D.; Lan, J.; Jenekhe, S. A.; Cao, G. Applications of Light Scattering in Dye-sensitized Solar Cells. *Phys. Chem. Chem. Phys.* **2012**, *14*, 14982-14998.

- (28) Baik, N. S.; Sakai, G.; Miura, N.; Yamazoe, N. Preparation of Stabilized Nanosized Tin Oxide Particles by Hydrothermal Treatment. *J. Amer. Ceram. Soc.* **2000**, *12*, 2983-2987.
- (29) He, Z.; Zhou, J. Synthesis, Characterization, and Activity of Tin Oxide Nanoparticles: Influence of Solvothermal Time on Photovoltaic Degradation of Rhodamine B. *Mod. Res. Catal.* **2013**, *2*, 13-18.
- (30) Rojo, A. G.; Berman, P. R. Rayleigh Scattering Revisited: From Glasses to Crystals. *Am. J. Phys.* **2010**, *78*, 1, 94-101.
- (31) Zuoli, H.; Wenxiu, Q.; Haixia, X.; Jing, C.; Yuan, Y.; Peng, S. Facile Synthesis of Self-sensitized TiO<sub>2</sub> Photocatalysts and Their Higher Photocatalytic Activity. *J. Am. Ceram. Soc.* **2012**, *95*, 12, 3941-3946.
- (32) Zhao, L.; Yu, J. Controlled Synthesis of Highly Dispersed TiO<sub>2</sub> Nanoparticles Using SBA-15 as Hard Template. *J. Colloid Interface Sci.* **2006**, *304*, 84-91.
- (33) Gratzel, M. Photoelectrochemical Cells. *Nature* **2001**, *414*, 338-344.
- (34) De Angelis, F.; Fantacci, S.; Mosconi, E.; Nazeeruddin, M. K.; Gratzel, M. Absorption Spectra and Excited State Energy Level of the N719 Dye on TiO<sub>2</sub> in Dye-sensitized Solar Cell Models. *J. Phys. Chem C* **2011**, *115*, 8825-8831.
- (35) Dahkhad, M.; Salavati-Niasari, M. Controlled Synthesis of Tin Dioxide Nanostructures via Two Simple Methods and the Influence on Dye-sensitized Solar Cell. *Electrochim. Acta* **2014**, *129*, 62-68.
- (36) Shang, G., Wu, J.; Tang, S.; Liu, L.; Zhang, X. Enhancement of Photovoltaic Performance of Dye-sensitized Solar Cell by Modifying Tin Oxide Nanorods with Titanium Oxide Layer. *J. Phys. Chem. C* **2013**, *117*, 4345-4350.

(37) Wali, Q.; Fakharuddin, A.; Ahmend, I.; Rahim, M. H. A.; Ismail, J.; Jose, R. Multiporous Nanofibers of SnO<sub>2</sub> by Electrospinning for High Efficiency Dye-sensitized Solar Cells. *J. Mater. Chem. A* **2014**, *2*, 17427-17434.